stoichiometry of the air–acetylene flames between the two portions of the experiment.

Interferences in the nitrous oxide–acetylene flames were measured at three stoichiometries: lean, medium, and rich. The curves varied considerably from each other, but not in any identifiable pattern; one stoichiometry did not appear to give "better" results than another. The data in the Figures 2–5 were taken from the medium flame.

CONCLUSIONS

The primary conclusion emerging from these experiments is that use of the air–acetylene flame burning on the single slot, flat-top burner produces the fewest interferences when determining copper, manganese, and nickel in acid media. Both the air–acetylene flame burning on a 3-slot head and the nitrous oxide–acetylene flame showed a greater tendency to exhibit interference effects, suggesting that these flames should be chosen with caution. For chromium the choice is not so clear. Both air–acetylene and nitrous oxide–acetylene flames produced roughly equivalent sensitivities and acid interferences. In this case the choice would be dependent on the presence of other possible interferences.

The interferences from hydrochloric and nitric acids were smallest indicating that these acids should be used if there is a choice of dissolution methods. However, if high accuracy is required, and the acid medium is other than dilute, standards should be made up in approximately matching concentrations of the same acid or acids.

Finally, it is clear that the design of the burner system has an important influence on analytical interferences, even within the general category of premix burners. The interferences found in this work are far smaller and less important than those reported in Reference *1*, in which a different premix burner system was employed.

RECEIVED for review August 6, 1971. Accepted November 23, 1971.

Double Modulation–Optical Scanning and Mechanical Chopping–in Atomic Absorption Spectrometry Using a Continuum Source

R. C. Elser and J. D. Winefordner[1]

Department of Chemistry, University of Florida, Gainesville, Fla. 32601

An atomic absorption flame spectrometer employing chopper modulated continuum radiation and wavelength modulation of radiation transmitted through the flame cell is described. The instrumental system does not respond either to Rayleigh scattering or to molecular absorption and emission processes occurring within the flame gases. Limits of detection of the order of 0.1 μg/ml and analytical curves linear over at least three orders of magnitude in concentration for Ag, Ca, Cd, Cr, Cu, Fe, Mg, and Ni are obtained. Expressions are derived to predict the response of the instrumental system to variation in experimental parameters and are verified experimentally.

ATOMIC ABSORPTION SPECTROMETRY has proved its utility as an analytical tool in the years since Walsh (*1*) introduced it. To the present time, the development of the technique has largely excluded the use of continua as sources. Several groups of workers (*2–6*) have realized the advantages of using a continuum source and have shown that it is practical. However, limits of detection have been poorer by a factor of 10 to 100 compared to those obtained using high intensity line sources. With a continuum source–medium resolution monochromator and low concentrations of absorber, the fraction of radiation absorbed by the absorption line is small as compared to the fraction absorbed with a line source. As a result, the signal due to the absorption line becomes buried in the noise of the continuum background and while the line may be discerned, its signal-to-noise ratio is low. It was thought that the weak absorption signal could be extracted from the noise and enhanced by using a derivative technique which has been employed successfully in other areas of spectrometry.

The technique of derivative spectrometry—*i.e.*, taking the derivative of the transmitted spectrum with respect to time or wavelength—was introduced in 1952 by French and discussed more fully in 1955 by Giese and French (*7*); they demonstrated its theoretical utility in resolving overlapping absorption bands having as much as 90% overlap. Collier and Singleton (*8*) applied the technique to infrared absorption spectra by taking the second derivative of the spectrum electronically; however, as Bonfiglioli and Brovetto (*9*) and Perregaux and Ascarelli (*10*) point out, analog differentiation of the detector output may actually degrade the signal-to-noise ratio of the derivative signal as compared to the original signal. Bonfiglioli and Brovetto (*9*) constructed a self-modulating derivative optical spectrometer which employed a vibrating mirror to modulate the image of the spectrum.

[1] Author to whom reprint requests should be sent.

(1) A. Walsh, *Spectrochim. Acta*, **7**, 108 (1955).
(2) W. W. McGee and J. D. Winefordner, *Anal. Chim. Acta*, **37**, 429 (1967).
(3) L. de Galan, W. W. McGee, and J. D. Winefordner, *ibid.*, p 436.
(4) J. D. Winefordner, V. Svoboda, and L. J. Cline, *CRC Crit. Rev. Anal. Chem.*, **1**, 233 (1970).
(5) V. A. Fassel, V. G. Mossotti, W. E. L. Grossman, and R. N. Kniseley, *Spectrochim. Acta*, **22**, 347(1966).
(6) J. H. Gibson, W. E. L. Grossman, and W. O. Cooke, *Proc. Feigl Anniv. Symp.*, 287 (1962).
(7) A. T. Giese and C. S. French, *Appl. Spectros.*, **9**, 78 (1955).
(8) G. L. Collier and F. Singleton, *J. Appl. Chem.*, **6**, 495 (1956).
(9) G. Bonfiglioli and P. Brovetto, *Appl. Opt.*, **3**, 1417 (1964).
(10) A. Perregaux and G. Ascarelli, *ibid.*, **7**, 2031 (1968).

They showed that by modulating the spectrum spatially and detecting at the appropriate frequency, the derivative of the transmitted spectrum was obtained; the signal-to-noise ratio of the derivative signal increased slightly as compared to the unmodulated signal. Their system proved efficacious in the analysis of complex molecular absorption bands (*11*) of rare earth nitrates in aqueous solutions.

Various ingenious techniques have been employed in obtaining a modulated spectrum. Stauffer and Sakai (*12*) used a rotating mirror stepped along one diameter to modulate the spectrum image by a discrete amount. Balslev (*13*) modulated the exit slit of his monochromator by mechanically linking it to a loudspeaker vibrating at 175 Hz. The derivative spectrum obtained was used to study the influence of stress on the indirect optical absorption edge in silicon and germanium crystals. Williams and Hager (*14*) also employed an oscillating exit slit to study the second derivative absorption spectra of gaseous atmospheric pollutants. Perregaux and Ascarelli (*10*) studied the first derivative absorption spectrum of I_2 in an incandescent lamp using a glass refractor plate to modulate the spectrum. In their system, the plate was epoxied to a steel ribbon which was oscillated by means of a piezoelectric bimorph. Shaklee and Rowe (*15*) used a fused silica refractor plate to modulate the reflectance spectra of InP and GaP at several temperatures. Snelleman *et al.* (*16*) modulated the emission spectra of elements in a flame using a quartz refractor plate and by operating in the second derivative mode were able to detect Ba in the presence of large amounts of Ca. The first application of derivative spectrometry to atomic absorption was by Snelleman (*17*) who used a mirror to scan the image of the dispersed spectrum across the exit slit of the monochromator. It was primarily his work which led to the development of the present system.

A continuum source and double modulation–*i.e.*, modulation of the radiation falling on the flame and emerging from it—was employed in this experimental system. Theoretical expressions are given to predict the response of the instrumentation to variation of experimental parameters. Several authors (*9*, *13–15*, *18*, *19*) have developed theoretical intensity expressions for derivative spectrometers. However, none have used their expressions as quantitative predictors of experimental signals. The derivation of theoretical expressions in this work closely parallels the derivations of Bonfiglioli and Brovetto (*9*) and Shaklee and Rowe (*15*). The quantitative predictions of the theory were investigated, and the system was used to construct analytical curves and limits of detection for eight elements: Ag, Ca, Cd, Cr, Cu, Fe, Mg, and Ni.

THEORETICAL CONSIDERATIONS

Mechanical Chopper Modulation. In atomic absorption spectrophotometry, it is important to eliminate any signal arising in the absorption cell which is not due to absorption of source radiation by analyte atoms. Because in most atomic absorption systems the absorption cell is a flame, there are four possible spurious sources of signal arising in the cell; emission due to flame gas combustion products; atomic emission and/or fluorescence of analyte atoms in the flame; Rayleigh scattering of source radiation by small unevaporated solvent droplets or other small particles; and molecular absorption by species arising from the flow gases and the sample matrix. Fortunately, in most cases, none of these has much effect upon the measured atomic absorption signal. Flame emission signals are discriminated against by modulation of the light source and utilization of a tuned ac amplifier. Atomic fluorescence signals would be impossible to discriminate against in atomic absorption measurements but fortunately fluorescence signals are generally negligible compared to absorption signals. However, Rayleigh scattering and molecular absorption of source radiation would increase the attenuation of the radiation passing through the flame and would be interpreted as an abnormally high concentration of absorbers in the flame. The effect of Rayleigh scattering and molecular absorption can be minimized by wavelength modulation.

The modulated source radiation, if it is focused on the chopper disk, is nearly square-wave modulated. However, in order to treat the system mathematically, it is convenient to assume that the source radiation is sinusoidally modulated. In this case, the modulated source spectral radiance at wavelength λ, $B^c(\lambda)$ in watts centimeter^{-2} steradian^{-1} nanometer^{-1}, may be expressed as

$$B^c(\lambda) = {}^1/_2 B^0(\lambda)[1 + \cos \omega_1 t], \qquad (1)$$

where $B^0(\lambda)$ is the unmodulated source spectral radiance (W cm^{-2} sr^{-1} nm^{-1}) at wavelength λ, ω_1 is the frequency of source modulation, in Hz, and t is time, in sec. In Equation 1, it is assumed that there are equally sized transparent and opaque sectors on the chopper disk. For consistency in this manuscript, normal parentheses ( ) following a symbol indicate that the parameter represented by the symbol is a function of the variables within the parentheses. Square brackets [ ] indicate multiplication of the terms within the brackets by the term(s) outside the brackets.

Refractor Plate Modulation. The wavelength modulation of the system is accomplished in this work by the use of an oscillating quartz plate. Because the index of refraction μ of the quartz plate is different from that of air, a beam of light incident on the plate will be refracted if its angle of incidence varies from 0°. The linear lateral displacement of the refracted beam may be expressed as

$$d = \tau \sin \alpha \left[1 - \frac{1}{\mu}\right] \qquad (2)$$

where d is the linear lateral displacement, in cm, of the entrance slit image at the exit focal plane, τ is the plate thickness, in cm, and α is the angle of incidence, in degrees, with respect to the normal to the surface.

For very small angles, sin α is approximately α, and the small angle approximation can be used. Therefore, the lateral displacement d becomes

$$d = \tau\alpha \left[1 - \frac{1}{\mu}\right] \qquad (3)$$

It is clear from this equation that the lateral displacement of the incident beam from the optical axis is proportional to the thickness τ of the refractor plate and to the angle α it makes with the incident beam. Also, because the image of the incident beam is displaced (for non-axial beams passing through

(11) G. Bonfiglioli, P. Brovetto, G. Busca, S. Levialdi, G. Palmieri, and E. Wanke, *Appl. Opt.*, **6**, 447 (1967).
(12) F. R. Stauffer and H. Sakai, *ibid.*, **7**, 61 (1968).
(13) I. Balslev, *Phys. Rev.*, **143**, 636 (1966).
(14) D. T. Williams and R. N. Hager, Jr., *Appl. Opt.*, **9**, 1597 (1970).
(15) K. L. Shaklee and J. E. Rowe, *ibid.*, p 627.
(16) W. Snelleman, W. C. Rains, K. W. Yee, H. D. Cook, and O. Menis, ANAL. CHEM., **42**, 394 (1970).
(17) W. Snelleman, *Spectrochim. Acta*, **23B**, 403 (1968).
(18) F. Aramu and A. Rucci, *Rev. Sci. Instrum.*, **37**, 1696 (1966).
(19) R. N. Hager, Jr., and R. C. Anderson, *J. Opt. Soc. Amer.* **60**, 1444 (1970).

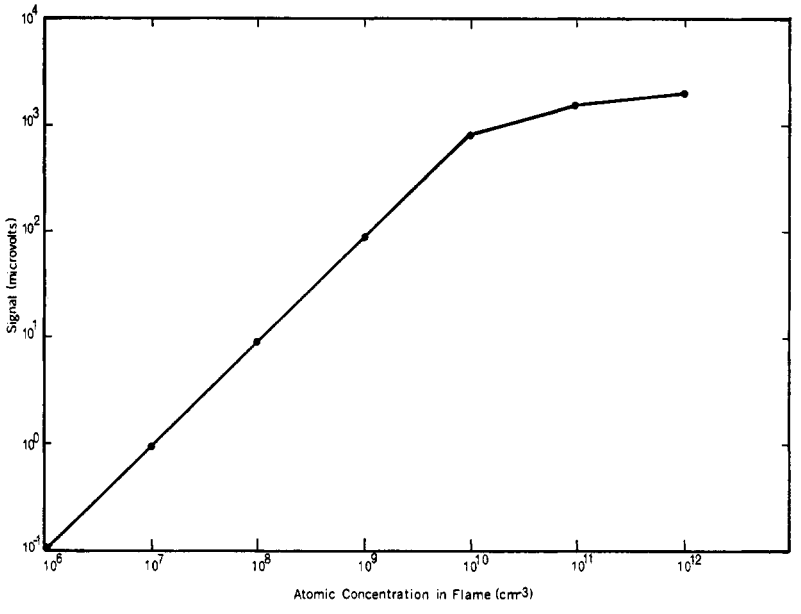

Figure 1. Theoretical curve of growth for Ca at 4227 Å by measurement of first derivative

the refractor plate) a small distance, a slight defocusing of the exit image results; fortunately, such defocusing is negligible in our case.

The lateral displacement of the image of the entrance slit at the exit slit plane in wavelength units, is

$$a = dR_d \tag{4}$$

where R_d is the reciprocal linear dispersion of the monochromator (nm cm^{-1}).

The result of oscillating the refractor plate periodically so that the angle of the incident beam varies periodically from α to $-\alpha$ at some regular frequency ω_2 is to oscillate the central wavelength of the entrance slit image (at the focal plane) about some mean wavelength, λ_c, which corresponds to the central wavelength emerging from the exit slit when the refractor plate is perpendicular to the entering light beam. The central wavelength, λ, of the mobile image with respect to the grating setting, λ_c, may be expressed as

$$\lambda = \lambda_c + a \sin \omega_2 t \tag{5}$$

where λ is the mean wavelength passing through the center of the exit slit, in nm.

The Rayleigh scattering and molecular absorption mentioned above is accounted for by wavelength modulation. Because Rayleigh scattering and molecular absorption are independent of wavelength over a small wavelength range, the transmitted signal will be the same at the absorption line and at wavelengths close by it. Thus, there will be a constant difference between the base-line signal and the absorption signal, whether scattering and/or molecular absorption are present or not.

Radiance Expressions. The first derivative input signal to the phase lock amplifier at frequencies $\omega_1 + \omega_2$ (or $\omega_1 - \omega_2$) assuming a dilute atomic gas has been derived in the Appendix and is given by

$$S_{\omega_1+\omega_2} = \frac{WH\Omega_M T_f \gamma R_L s a B^0(\lambda) \rho k_0 l \exp[-1/2] \exp[-\bar{k}_\lambda l]}{2\sqrt{2}\,\Delta\lambda} \tag{6}$$

and the second derivative input signal to the phase lock amplifier at frequency $\omega_1 + 2\omega_2$ (or $\omega_1 - 2\omega_2$) assuming a dilute atomic gas which has also been derived in the Appendix is given by

$$S_{\omega_1+2\omega_2} = \frac{WH\Omega_M T_f \gamma R_L s a^2 B^0(\lambda) \rho k_0 l \exp[-\bar{k}_\lambda l]}{8\Delta\lambda^2} \tag{7}$$

where W and H are the width and height of the monochromator slit, respectively, in cm, Ω_M is the solid angle of radiation collected by the monochromator in sr, T_f is the transmission factor (no units) of the optics of the system, γ is the phototube radiant sensitivity in AW^{-1}, R_L is the phototube load resistor, in Ω, s is the spectral bandwidth of the monochromator, in nm, and a and $B^0(\lambda)$ have already been defined, ρ is a factor (no units) to account for the effect of the spectral bandwidth of the monochromator upon the measured absorption coefficient, k_0 is the peak atomic absorption coefficient for an absorption line broadened purely by Doppler broadening, l is the absorption path length of the flame cell, k_λ is a modified atomic absorption coefficient at wavelength λ (see Appendix) and $\Delta\lambda$ is the apparent half-width of the measured spectral line (see Appendix).

The ratio of the first derivative signal $S_{\omega_1+\omega_2}$ to the second derivative signal $S_{\omega_1+2\omega_2}$ is obtained by dividing Equation 6 by Equation 7 and is given by

$$\frac{S_{\omega_1+\omega_2}}{S_{\omega_1+2\omega_2}} = \left[\frac{2\Delta\lambda\sqrt{2}}{a}\right] \exp\left[-\frac{1}{2}\right] \tag{8}$$

Equations 6 and 7 are useful expressions for predicting the shape of the curves of growth for the derivative system. A theoretical (obtained using Equation 6) first derivative growth curve is shown in Figure 1.

Balslev (*13*) has shown that there is an optimum spectral modulation amplitude; the resolution for a conventional dispersive monochromator is $\frac{s_1 + s_2}{2} = s$, where s_1 and s_2 are the spectral slit widths of the entrance slit and exit slit, respectively. For the case of a monochromator modified to produce a derivative signal and having a spectral modulation amplitude, a, the resolution is

$$\frac{s_1 + s_2 + a}{2} = s \tag{9}$$

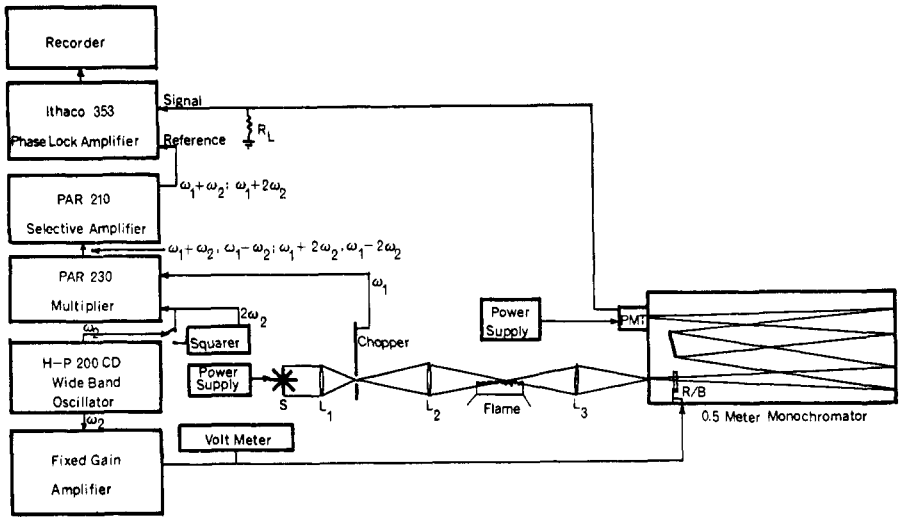

Figure 2. Block diagram of experimental system for double-modulation optical scanning atomic absorption spectrometer with a continuum source

Because the signal of the derivative spectrometer, according to Balslev, is proportional to $s_1 s_2 a$, the best choice for slit widths and modulation amplitude for optimum resolution and signal is $s_1 = s_2 = a$. In the derivation given in the Appendix, it is assumed that $s_1 = s_2$. Considering now the size of a, one sees that if $a < s_1$, resolution will be improved but the signal will decrease, and if $a > s_1$, the signal will increase but resolution will suffer. For the optimum case, a should be chosen equal to s_1; from Equation 8 the ratio of the first to second derivative signals is then 1.7 (*i.e.*, $a \cong \Delta\lambda$).

Limits of Detection. Winefordner and Vickers (20) have derived expressions for calculating the theoretical concentration of analyte at the limit of detection in atomic absorption flame spectrometry for a system employing a hollow cathode discharge lamp as a source and dc detection of the signal. In their derivation, they defined the limit of detection as the concentration of analyte atoms in a flame which produces a change in signal equal to twice the root-mean-square noise signal due to all sources of noise present in the system. The major sources of noise present in any system are: fluctuations in the signal arising from the photodetector or photon noise; fluctuations in signal arising from source intensity fluctuations or source flicker noise; fluctuations in the signal arising from fluctuations in the intensity of background flame emission intensity or flame flicker noise. Of these sources of noise, flame flicker and source flicker noises are of the "pink" or $1/f$ variety at low frequencies (less than 100 Hz) but are "white" at higher frequencies—*i.e.*, the spectral noisepower is approximately constant over the entire frequency spectrum. Photon noise, however is "white" at all frequencies and should be the dominant source of noise for an atomic absorption spectrometer utilizing a continuum source and an ac detection system operating at a frequency greater than about 100 Hz (*17*). The following derivation of the analyte concentration at the limit of detection is based on the assumption that the system is photon noise limited. The photoanodic current due to photon noise may be written (*20*) as

$$\overline{\Delta i_p} = [2BMe\Delta f\gamma WH\Omega_M T_f B^0(\lambda)s]^{1/2} \qquad (10)$$

where B is a factor characteristic of the photodetector dynodes, M is the multiplication (amplification) factor of the photodetector (no units), e is the charge on the electron, in C, Δf is the frequency response bandwidth, in Hz, and all other terms have been previously defined. Because photon noise is frequency independent, it will be detected along with the signal. At the limit of detection, the limiting S^l due to analyte absorbing species will be equal to twice the photon noise. For the first derivative system

$$S_{\omega_1+\omega_2}{}^l = 2R_L\overline{\Delta i_p} \qquad (11)$$

The term in the signal expression (Equation 6) which related the signal size to the number of analyte absorbers is k_0. The limiting detectable atomic absorption coefficient, $k_0{}^l$ for the limiting detectable number of atoms in the flame, $n_i{}^l$ is given (*21*) by

$$k_0{}^l = \frac{2\sqrt{\ln 2}\ \lambda_0^2\ \pi e^2 n_i{}^l f}{\sqrt{\pi}\Delta\lambda_D mc^2} \qquad (12)$$

where $n_i{}^l$ is the limiting detectable number of atoms in the ith state per cm^3 of flame gases, $\Delta\lambda_D$ is the Doppler half-width, in nm, f is the absorption oscillator strength for the atomic transition (no units) and c is the speed of light in cm sec^{-1}; $n_i{}^l$ may be calculated using the Boltzmann equation (*20*) and is

$$n_i{}^l = \frac{n^l g_i}{Z(T)} \qquad (13)$$

where n^l is the total number of atoms in all states at the limit of detection, in cm^{-3}, g_i is the statistical weight (no units) of state i; and $Z(T)$ is the electronic partition function (no units) of the atom; $Z(T) = \Sigma g_j \exp[-E_j/kT]$, where E_j is the energy of state j above the ground state in eV, k is the Boltzmann constant in eV °K^{-1}, T is the absolute temperature in °K, and the summation is over all electronic states of the atom.

Equations 6, 10, 12, and 13 may be substituted into Equation 11, and the resulting expression solved for n^l to yield a general equation for the limiting number of atoms detectable per cm^3 of flame gases.

$$n^l = \left[\frac{[Z(T)]}{g_i}\right]\left[\frac{2\Delta\lambda_D c}{\left[\frac{\pi e^2}{mc}\right]\rho\ \lambda_0^2 fl\ \exp\left[-\frac{1}{2}\right]}\right] \cdot \left[\frac{2\pi BMe\Delta f}{[\ln 2]WH\Omega_M T_f B^0(\lambda)s\gamma}\right]^{1/2} \qquad (14)$$

The limiting detectable number of atoms per cm^3 of flame gases, n^l, can be converted to limiting detectable solution con-

(20) J. D. Winefordner and T. J. Vickers, ANAL. CHEM., **36**, 1947 (1964).

(21) A. C. G. Mitchell and M. W. Zemansky, "Resonance Radiation and Excited Atoms," 2nd ed., 1961, Cambridge University Press, New York, N.Y.

Table I. Optical Components

Component	Type and/or description	Supplier
Source	Model 150X8S, 150-watt xenon arc with parabolic silver reflector, collimated beam	Varian, Eimac Div., 301 Industrial Way, San Carlos, Calif.
	Type FCS, 105-watt tungsten–halogen lamp operated at 24 volts	General Electric Co., Photo Lamp Dept., Nela Park, Cleveland, Ohio
Xenon arc source power supply	Model P 250S-2, Illuminator Power Supply	Varian, Eimac, Div., 301 Industrial Way, San Carlos, Calif.
Tungsten-halogen lamp power supply	Type CVN-1, Constant voltage transformer	Sola Electric Co., Elk Grove Village, Ill.
	Class A, Type 1 24-volt, 10-amp step-down transformer	Freed Transformer Co., Inc., Brooklyn, N.Y.
Nebulizer	Type 303-0110 adjustable nebulizer and mixing chamber	Perkin-Elmer Corp., Norwalk, Conn.
Burner	Type 303-0401 three-slot Boling burner	Perkin-Elmer Corp., Norwalk, Conn.
Monochromator	Type 82-000, 0.5-meter Ebert mount scanning monochromator with bilateral adjustable curved slits	Jarrell-Ash Corp., 590 Lincoln St., Waltham, Mass.
Grating	Type 13701, 1180 grooves/mm, 52 mm × 52 mm, blazed at 5000 Å	Jarrell-Ash Corp., 590 Lincoln St., Waltham, Mass.
Lenses	2-inch diameter, bi-convex Spectrosil lenses with the following focal lengths L1 = 3.2 inches L2 = 2.4 inches L3 ± 2.7 inches	Esco Products, Oak Ridge, N.J.
Refractor plate	Suprasil quartz plate, 1.5 inches × 0.5 inch × 0.125 inch	Esco Products, Oak Ridge, N.J.
Piezoelectric bimorph	Type PZT − 5, 1.25 inches × 0.5 inch × 0.021 inch	Gould, Inc., Piezoelectric Division, 232 Forbes Road, Bedford, Ohio

Table II. Electrical Components

Component	Type and/or description	Supplier
Wide band oscillator	Model 200 CD Wide Band Oscillator	Hewlett-Packard Co., 1501 Page Mill Rd., Palo Alto, Calif.,
Multiplier unit	Model 230, Multiplier Unit, A × B mode	Princeton Applied Research Corp., Princeton, N.J.
Squarer	Model 426 Wide Band Four Quadrant Multiplier-Divider Square Rooter powered by Model 904 Dual Op Amp Power Supply	Analog Devices, Cambridge, Mass.
Selective amplifier	Model 210, Selective Amplifier	Princeton Applied Research Corp., Princeton, N.J.
Phase-lock amplifier	Model 353 Phase Lock Amplifier with Type B1 Amplifier, C1 Demodulator, and Display Module	Ithaco, Inc., 413 Taughannock Blvd., Ithaca, N.Y.
Multiplier phototube	RCA 1P28A having S-5 response operated at −800 volts	Heath Co., Benton Harbor, Mich.
Phototube power supply	Model 26-770 High Voltage Power Supply	Jarrell-Ash Corp., 590 Lincoln St., Waltham, Mass.
Recorder	Model SR 10-inch chart recorder with 10 mV adapter, 3-speed drive	Sargent-Welch Scientific Co., 3125 7th Avenue, Birmingham, Ala.

centration, in μg ml^{-1}, C^l, by use of the following equation (*20*).

$$C^l = \frac{3.3 \times 10^{-19} n^l T Q n_T A}{\phi \epsilon \beta n_{298}} \quad (15)$$

where T is the flame temperature, in °K, n_T is the number (no units) of moles of combustion products at temperature T, n_{298} is the number (no units) of moles present at 298 °K, Q is the flow rate of unburned gases, in cm^3 sec^{-1} at room temperature and one atmosphere pressure, ϕ is the flow rate of solution in cm^3 min^{-1}, ϵ is the efficiency of vaporization and nebulization processes (no units), β is a factor to account for atomic losses due to incomplete dissociation and ionization (no units), and A is the atomic weight of the analyte, in grams mole^{-1}. The constant (3.3×10^{-19}) contains the numerical factors 298 °K, Avogadro's number, and conversion factors from minutes to seconds and from grams to micrograms. It

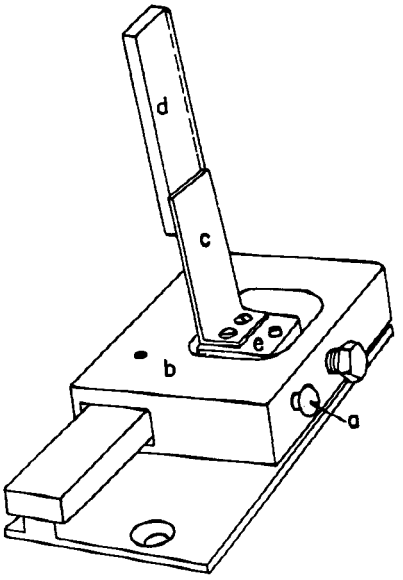

Figure 3. Electrode holder for piezoelectric transducer

Key: a = brass holder; b = brass holder block; c = piezoelectric bimorph transducer; d = quartz refractor plate; e = Teflon insulator block

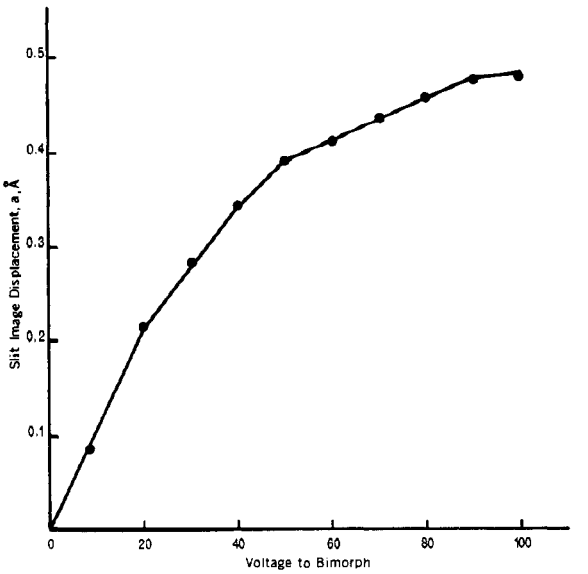

Figure 4. Spectral modulation amplitude (slit image displacement) *vs.* voltage supplied to the bimorph

thus has units of (moles atom^{-1}) (seconds minute^{-1}) (micrograms gram^{-1}) ($^{\circ}$K^{-1}).

Signal-to-Noise Ratio. The signal-to-noise ratio of the system in the first derivative mode for a dilute atomic gas is obtained by dividing Equation 6 by Equation 10 and simplifying

$$S/N = \left[\frac{WH\Omega_M T_f B^0(\lambda)\gamma BMe\Delta fs}{4}\right]^{1/2} \cdot \left[\rho k_0 l \exp\left[-\frac{1}{2}\right] \exp[-\bar{k}_\lambda l]\right] \quad (16)$$

Equation 16 predicts that the signal-to-noise ratio will improve with the square root of the source spectral radiance at the wavelength of measurement.

EXPERIMENTAL SYSTEM AND PROCEDURES

A block diagram of the instrumental system is given in Figure 2. The entire system was mounted on a 1-inch thick steel plate using quick-release magnetic mounts. Components used in the system are listed in Tables I and II.

The quartz refractor plate used to displace the image of the entrance slit was mounted in a brass electrode holder as shown in Figure 3. The electrode holder was located on the monochromator chassis at a distance from the entrance slit such that the width of the plate was sufficient to totally intersect the solid angle of radiation collected by the collimator mirror. The refractor plate was epoxied to a piezoelectric bimorph. Oscillation of the refractor plate was accomplished by supplying the piezoelectric bimorph with a sinusoidally varying voltage. The optimum performance of the piezoelectric bimorph was expected to occur at its resonance frequency. The approximate resonance frequency, ω_2, was calculated (*22, 23*) using

$$\omega_2 = \frac{2257}{L^2} \quad (17)$$

where L is the free length of the vibrating member, in cm. For our system, ω_2 was 56 Hz. Experimentally the resonance frequency was found to be 55 Hz. Consequently, the bimorph was driven at 55 Hz by a voltage of the appropriate magnitude to attain the desired deflection and thereby the desired spectral modulation interval (see Figure 4).

The driving voltage to the piezoelectric bimorph was supplied at the proper frequency by using a variable amplitude, wide-band oscillator feeding into a fixed-gain power amplifier which was capable of supplying up to 120 V (rms) without distortion of the output waveform. (A suitable commercial amplifier would be the Model DCA-10, Krohn-Hite Power Amplifier, Krohn-Hite Corp., 580 Massachusetts Ave., Cambridge, Mass.)

The reference signal of the piezoelectric transducer frequency, ω_2, was taken at the oscillator output. When the system was operated in the first derivative mode, the sample signal and the reference signal from the mechanical chopper were used as inputs to a multiplier. The result of multiplying two periodic functions together is given by

$$[\sin a][\cos b] = {}^1/_2[\sin[a + b] + \sin[a - b]] \quad (18)$$

In order to differentiate between the sum and difference frequencies in the multiplier output, a tuned amplifier of high Q was used to select the proper frequency to be used as the reference signal to the lock-in. For the first derivative spectrum, the sum frequency was 313 Hz, and the difference frequency was 203 Hz (ω_1 was 258 Hz).

For operation of the system in the second derivative mode, the reference signal from the oscillator was fed into a squarer to obtain a signal at twice the oscillator frequency, 2 ω_2. The outputs of the squarer and the chopper reference signal were fed into the multiplier as for first derivative operation and the selective amplifier tuned appropriately to either 368 Hz ($\omega_1 + 2\omega_2$) or 148 Hz ($\omega_1 - 2\omega_2$).

Solutions. Solutions of each element to be analyzed were prepared from reagent grade chemicals. Stock solutions for Ag, Ca, Cd, Cr, Cu, Fe, Mg, and Ni were made from $AgNO_3$, $Ca(C_2H_3O_2)_2 \cdot H_2O$, $CdCl_2 \cdot 2^1/_2H_2O$, $K_2Cr_2O_7$, $CuSO_4 \cdot 5H_2O$, $FeSO_4 \cdot 7H_2O$, $MgSO_4$, and $NiSO_4 \cdot 6H_2O$, respectively. Three solutions of relative concentration 1.00, 0.50 and 0.25 were prepared for each decade of concentration examined. All

(22) L. D. Landau and E. M. Lifshitz, "Theory of Elasticity," Addison-Wesley Publishing Co., Reading, Mass., 1959.
(23) Bulletin PD-9247, Gould Inc., Piezoelectric Division, 232 Forbes Road, Bedford, Ohio, 1969.

Table III. Verification of Theory

Experiment	Conditions	Predicted results	Experimental results
Signal *vs.* spectral modulation amplitude at constant slit width	10 μg ml^{-1} Ca aspirated, 25-μ slit = 0.40 Å	Maximum signal at 0.40 Å	Maximum signal at 0.41 Å
Comparison of magnitudes of 1st and 2nd derivative signals	Conditions identical for both. 10 μg ml^{-1} Ca aspirated. Spectral modulation interval equal to spectral bandwidth	Ratio of $\frac{1st}{2nd}$ = 1.7	Ratio of $\frac{1st}{2nd}$ = 1.4
Comparison of normal AAC with 1st derivative AAC	25 μg ml^{-1} Ca aspirated. All instrumental parameters identical for both cases	Normal AA signal 7.7 mV Derivative signal 3.3 mV	Normal AA signal 15.6 mV Derivative signal 3.3 mV
Verification of photon noise limitation	1 μg ml^{-1} Ca aspirated. Xenon (X) arc *vs.* tungsten–halogen (T) lamp	$\frac{(S/N)_X}{(S/N)_T}$ = 0.3	$\frac{(S/N)_X}{(S/N)_T}$ = 0.5
Detection at sum and difference frequencies for 1st derivative	5.0 μg ml^{-1}, 1.0 μg ml^{-1} and 0.5 μg ml^{-1} Cu measured at 313 Hz and 203 Hz	Sum = difference	50 μg ml^{-1}. Sum = 1872 μV; difference = 1916 μV. 1.0 μg ml^{-1}. Sum = 420 μV; difference = 420 μV. 0.5 μg ml^{-1}. Sum = 225 μV; difference = 213 μV

solutions were prepared as aqueous solutions using high quality deionized water.

Experimental Procedure. The source was run at 12 amperes and 12.5 volts dc. The spectral bandwidth, s, and the spectral modulation amplitude, a, were maintained at a ratio of 1. The actual spectral bandwidth used in the experiments varied between 0.03 nm and 0.05 nm. The slit height was kept at 0.2 cm. Data for analytical curves (see Figure 5) were taken with the monochromator in the nonscanning mode. The wavelength was set manually to give the maximum signal deflection on the recorder. Thermal drift of the monochromator away from the preset wavelength did not prove to be a problem, and an entire set of data could be collected without the necessity for readjustment of the monochromator. A nearly stoichiometric acetylene–air flame was used for all analyses except for Ca and Cr for which a fuel-rich flame was used.

RESULTS AND DISCUSSION

Verification of Theory. Various experiments were performed to test the validity of the theoretical expressions derived above. The results of these are discussed below and summarized in Table III.

Optimum Slit Width to Modulation Amplitude Ratio. The experiment to determine the optimum spectral bandwidth to spectral modulation amplitude ratio to verify Balslev's prediction (*13*) involved using a set of fixed straight slits of spectral bandwidth 0.40 Å. The signal resulting from the aspiration of a solution of 10 μg ml^{-1} Ca into the flame was measured as a function of spectral modulation amplitude. The results are plotted in Figure 6. The theoretical optimum and the experimental optimum agree within about 3%.

First Derivative Mode *vs.* Second Derivative Mode. Equation 8 predicts that when the spectral modulation interval is equal to the spectral bandwidth, the ratio of the magnitudes of the first and second derivative signals is equal to 1.7. An experiment was performed at three different slit widths but at the same a/s ratio of unity. The mean ratio was found experimentally to be 1.4.

Normal AAC Compared with Derivative AAC. Comparisons of different analytical techniques are usually not valid because one experimentalist may compare results obtained with his system to those obtained in another laboratory under different conditions with different instrumentation in many cases. A more fair comparison is to perform both analytical techniques under the same laboratory conditions with as many common pieces of instrumentation as possible. In this manner, differences which arise may be attributed to the differences in techniques. To this end, both normal atomic absorption spectrometry with a continuum source (AAC) and a mechanical chopper and derivative AAC were performed with the same instrumentation. All experimental conditions, slit width and height, source power, flame conditions, and analyte concentrations were identical for both techniques. The only difference between the techniques was oscillation of the refractor plate in the derivative technique.

The signals predicted by theory for normal AAC (*20*) and for the first derivative signal by Equation 6 for 25 μg/ml^{-1} of Ca were calculated and compared with experimental values. The results are listed in Table III and are in good agreement. Furthermore, even though the signal magnitude for normal AAC was five times larger than for the first derivative AAC signal, the S/N ratio was about five times poorer.

Direct comparison of results obtained with the present system with the best previous results by normal AAC (*5*) were unfavorable to the derivative system. However, the systems were different enough that the arguments raised in the first paragraph apply. When comparison was made on equal terms—*i.e.*, using ethanolic solutions of analyte and the same instrumentation—the derivative system proved to have an advantage in S/N ratio.

Photon Noise Limitation. The signal-to-noise and limiting detectable concentration expressions derived above have been based on the assumption that photon noise is the limiting noise in the present system (*17*). Equation 16 predicts that for all other parameters being constant, S/N should vary as the square root of the source radiance, $B^0(\lambda)$. By using two

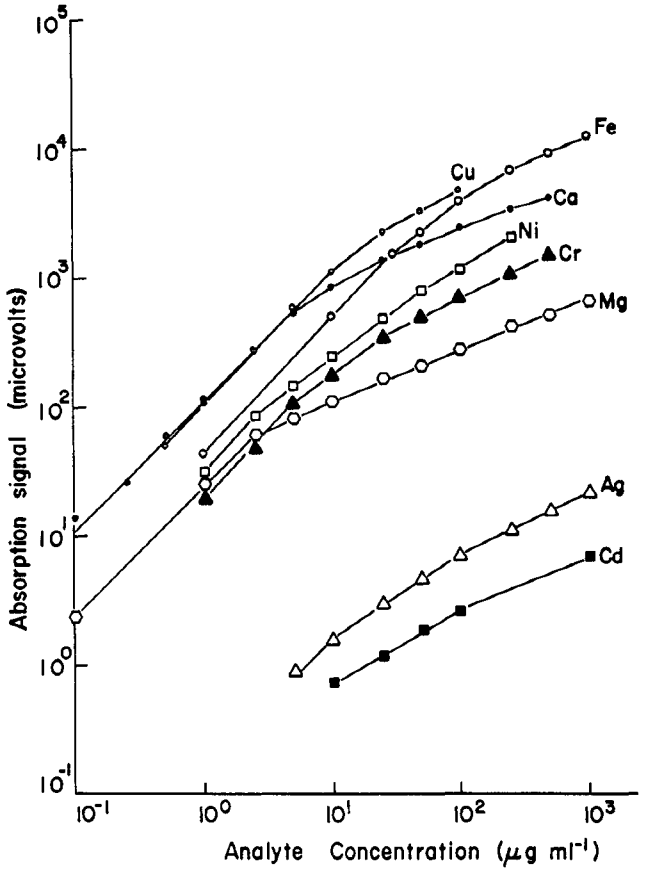

Figure 5. Analytical absorption curves for Ag, Ca, Cd, Cr, Cu, Fe, Mg, Ni

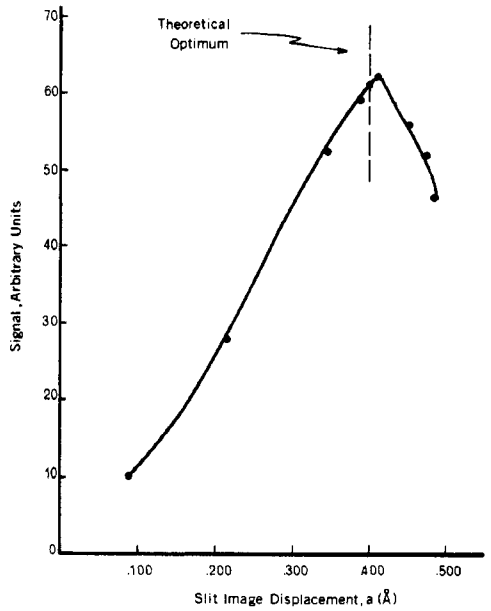

Figure 6. First derivative signal *vs.* spectral modulation amplitude (slit image displacement) at constant spectral bandwidth of 0.40 Å

sources, the ratio of whose radiances is known, one can verify the prediction of Equation 16. Writing Equation 16 for the two sources and taking the ratio results in the following expression

$$\frac{(S/N)_T{}^1}{(S/N)_X} = \left(\frac{W_T H_T B^0(\lambda)_T s_T}{W_X H_X B^0(\lambda)_X s_X}\right)^{1/2} \qquad (19)$$

Table IV. Limits of Detection

Element	Analytical line, nm	Theoretical[a] C^l μg ml^{-1}	Actual C^l μg ml^{-1}
Cadmium	228.8	5	10
Magnesium	285.2	2×10^{-2}	10^{-1}
Copper	324.7	7×10^{-2}	5×10^{-1}
Silver	328.1	2×10^{-1}	2
Nickel	341.4	—	2
Chromium	357.9	4×10^{-1}	4×10^{-1}
Iron	371.9	2×10^{-1}	4×10^{-1}
Calcium	422.7	1×10^{-1}	1×10^{-1}

[a] The free atom fraction β, the flame gas expansion factor, $n_T T/n_{298}$ and efficiency of nebulization factors, ϵ, were taken from de Galan and Samaey (*24*) for the various elements in an C_2H_2/air flame [the flames gases were adjusted to be identical to those used by de Galan and Samaey (*24*) in their studies]. The statistical weights and oscillator strengths for the transition were taken from Mavrodineanu and Boiteux (*25*). The electronic partition functions were taken from de Galan, Smith, and Winefordner (*26*). The solution flow rate ϕ, flame gas path length l, and gas flow rate ϕ were measured parameters. The Doppler half-width $\Delta\lambda_D$ was calculated (*27*) for each atom in the specific flame used by us. The monochromator spectral bandwidth, s, was selected for optimal response (see Figure 6). The monochromator slit width W and height H were read from the respective dials. The monochromator solid angle Ω_m and transmission factor T_f were estimated from the focal length and area of the collimator and from the number and characteristics of the optical surfaces available in the optical system. The photodetector anodic sensitivity factor γ was estimated by means of a calibrated source and the frequency interval Δf was estimated from the time constant of the phase sensitive amplifier. The dynode factor B was estimated from manufacturers data for the RCA 1P28 photomultiplier tube.

Experimentally, tungsten-iodine, T, and xenon, X, lamps were used as the sources and had a radiance ratio of 0.16 at the wavelength of measurement, 4227 Å. A 1 μg ml^{-1} solution of Ca was used as the experimental probe. The ratio calculated from the appropriate experimental parameters was 0.3 while the experimentally determined ratio was found to be 0.5.

Frequency of Detection. The first derivative signal should appear at both the sum and difference frequencies (see Appendix). The measurement of three concentrations of Cu (5.0 μg ml^{-1}, 1.0 μg ml^{-1}, and 0.5 μg ml^{-1}) was carried out at the sum and difference frequencies. The results are tabulated in Table III and are in close agreement.

Limits of Detection. The theoretical limits of detection calculated using Equation 15 and the experimentally measured limits of detection are tabulated in Table IV. Experimental limits of detection were obtained by extrapolating the analytical curves to the concentration where the signal was equal to twice the rms noise.

Because the derivative spectrometer is sensitive to small, but abrupt, changes in the slope of the spectrum it views, both the source and flame background spectra were examined over an interval of 0.5 nm on either side of the analytical lines used. In all cases, the source background varied linearly and had no fine structure in its spectrum. In the cases of Mg, Cr, and Fe, there were some flame emission lines within the 1-nm

(24) L. de Galan and G. F. Samaey, *Spectrochim. Acta*, **25B**, 245 (1970).
(25) R. Mavrodineanu and H. Boiteux, "Flame Spectroscopy," John Wiley, New York, N.Y., 1965.
(26) L. de Galan, R. Smith, and J. D. Winefordner, *Spectrochim. Acta*, **23B**, 521 (1968).
(27) M. L. Parsons, W. J. McCarthy, and J. D. Winefordner, *Appl. Spectrosc.*, **20**, 223 (1966).

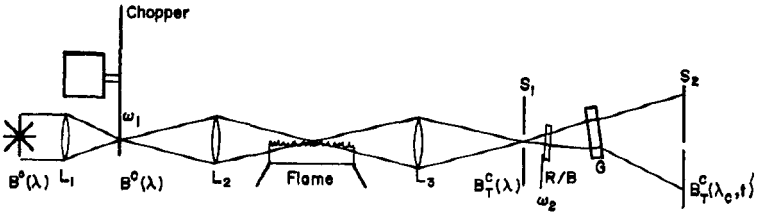

Figure 7. Schematic diagram of the optical system

interval, but these were far enough away from the analytical lines not to interfere.

It should be noted that the general shape of all analytical curves follows that of the theoretical curve of growth in Figure 2, having a slope of 1 at low concentrations and a slope of less than 1 at concentrations greater than 10 μg ml^{-1} (corresponds approximately to an atomic concentration in the flame of 10^{10} atoms cm^{-3}).

CONCLUSIONS

The advantages of using a continuum source in atomic absorption spectrometry *vs.* line sources have been enumerated (*2–6*). In addition to the cost and time-saving advantages, one further important capability is apparent. With line sources, the analyst is generally restricted to resonance transitions—*i.e.*, transitions arising from the ground state—because these are usually the most strongly emitted lines of the source. However, in certain cases, *e.g.*, Ni and Fe, there are very low lying states having large transition probabilities which may be appreciably populated at the temperature of the flame. Systems employing continuum sources may take advantage of these more favorable transitions while those using line sources generally may not.

It was shown in Table III that the signal obtained for identical concentrations of analyte was larger for normal mode AAC than for the first derivative mode AAC by a factor of about 5, whereas the signal-to-noise ratio of the derivative mode is 5 times that of the normal mode. In addition, if the absorption peak happens to be superimposed on a slowly increasing or decreasing background, no background base-line correction need be applied because the first derivative of such a slope is a constant.

The advantage of using double modulation over wavelength modulation as in Snelleman's system (*17*) is that all of the signal arising from the flame due to emission is totally rejected. In addition, with a piezoelectric transducer to drive the refractor plate, the instrumental system can be converted to the normal mode by simply turning off the oscillation of the refractor plate.

An additional capability of the system allows first or second derivative operation in the emission modes, as in Snelleman *et al.* (*16*), by simply turning off the source and chopper and detecting at ω_2 or $2\omega_2$ for the first or second derivative signal, respectively.

The system which has been described is a prototype and was designed to test and verify the theory derived for it. As a result, limits of detection which were obtained in no way present the ultimate which might be realized by a system of this type. The chief limitation has been the insufficient spectral radiance of the source employed. Presently, work is continuing to improve the system. A source of higher spectral radiance is being included as well as the substitution of mirrors for lenses to increase the transmission of light throughout the optical system.

APPENDIX
DERIVATION OF RADIANCE EXPRESSIONS

The experimental arrangement for which the first and second derivative radiance expressions are derived is illustrated in Figure 7. The source employed must be continuum for the expressions to hold. The source radiance and the radiance at each important point in the system are also indicated in Figure 7.

The continuum source spectral radiance, $B^0(\lambda)$, is focused onto the blade of a chopper wheel rotating at an angular frequency ω_1. The modulated spectral radiance, $B^c(\lambda)$, is then focused onto a flame absorption cell into which atomic absorbing species of the analyte may be introduced. The radiance transmitted through the absorption cell, $B_T^c(\lambda)$, is related to the incident radiance, $B^c(\lambda)$, by the absorption law (*3, 20*) and is

$$B_T^c(\lambda) = B^c(\lambda) \exp [-\bar{k}_\lambda l] \quad (20)$$

where $\bar{k}_\lambda$ is a modified atomic absorption coefficient evaluated at wavelength λ, in cm^{-1} and l is the path length of the flame, in cm. When a medium resolution monochromator (as in this case) having spectral bandwidths equal to or larger than the half-width, $\Delta\lambda_A$, of the absorption line (*21*) is used, the apparent half-width, $\Delta\lambda$, of the spectral profile viewed by the monochromator is approximately the same as the spectral bandwidth, s, (*28*). The apparent half-width, $\Delta\lambda$, is herein defined as

$$\Delta\lambda = [s^2 + \Delta\lambda_A{}^2]^{1/2} \quad (21)$$

The spectral bandwidth, s, of the monochromator is given by

$$s = R_d W \quad (22)$$

where W is the slit width of the monochromator (cm) and R_d is the reciprocal linear dispersion of the monochromator, in nm cm^{-1}. Kostkowski and Bass (*29*) have calculated the change in the absorption coefficient for various spectral bandwidth-to-absorption line half-width ratios; for ratios greater than 2, which is generally the case for real analytical situations involving atomic lines, the observed peak value of the absorption coefficient varies from 75% to less than 50% of k_0, the peak absorption coefficient for a line broadened by purely Doppler broadening. Therefore, $\bar{k}_\lambda$ may be expressed as

$$\bar{k}_\lambda = \rho k_0 \exp -\left[\frac{\lambda - \lambda_0}{\Delta\lambda}\right]^2 \quad (23)$$

where ρ is a coefficient less than 1.0 to account for the diminution of the atomic absorption coefficient due to the finite spectral bandwidth of the monochromator and λ_0 is the wavelength at the center of the absorption line profile. This expression only approximates reality because of the assumption of a line having a Gaussian type of profile. However, by considering the line as having a Gaussian shape instead of its true shape (Voigt profile) which results from the several

(28) S. S. Penner, "Quantitative Molecular Spectroscopy and Gas Emissivities," Addison-Wesley Publishing Co., Reading, Mass., 1959.

(29) H. J. Kostkowski and A. M. Bass, *J. Opt. Soc. Amer.*, **46**, 1060 (1956).

broadening processes occurring in flames, the expression becomes amenable to mathematical treatment and does not result in appreciable errors in the treatment. Equation 20 may be rewritten in a form which indicates more clearly that the exponential term simply expresses the transmission of the flame cell as a function of wavelength λ.

$$B_T^c(\lambda) = B^c(\lambda)T(\lambda) \tag{24}$$

The radiance transmitted through the absorption cell is focused upon the entrance slit of a monochromator after which it passes through a refractor plate modulated at an angular frequency ω_2. The effect of the displacement of the image is to cause the spectrum produced by the grating of the monochromator to periodically oscillate about a mean wavelength, λ_c, corresponding to the central wavelength of the spectral band of radiation emerging from the exit slit when the monochromator is used in the conventional mode. The wavelength λ of the oscillating spectrum which is viewed by the center of the exit slit at any time t is given by Equation 5. Therefore, the radiation emerging from the exit slit of the monochromator, $B_T^c(\lambda_c,t)$, is a function of the periodic oscillation of the spectrum about the center of the exit slit. As a result of the finite width of the exit slit, $B_T^c(\lambda_c,t)$ is also a function of the spectral bandwidth of the monochromator. The modulated spectrum passing the exit slit may be expressed in the form of an integral of $B_T^c(\lambda_c,t)$ convoluted with the slit function of the monochromator, $S(\lambda)$, evaluated over the spectral bandwidth of the monochromator.

$$B_T^c(\lambda_c,t) = \int_{\lambda_c-s/2}^{\lambda_c+s/2} B_T^c(\lambda)S(\lambda)\mathrm{d}X \tag{25}$$

where X is $\lambda - \lambda_c$.

In the case of a monochromator having equal entrance and exit slits and equivalent optical components for the collimator and decollimator—*i.e.*, unity magnification within the monochromator—$S(\lambda)$ is a triangular function and is expressed as

$$\begin{aligned} S(\lambda) &= 1 - \frac{|X|}{s}, \quad |X| = |\lambda - \lambda_c| < s \\ S(\lambda) &= 0, \qquad |X| = |\lambda - \lambda_c| \gtrsim s \end{aligned} \tag{26}$$

$B_T^c(\lambda)$ as expressed by Equation 24 may be rewritten as a function of the modulated spectrum and the slit width.

$$B_T^c(\lambda) = B^c(\lambda_c + \sin\omega_2 t + |X|)T(\lambda_c + a\sin\omega_2 t + |X|) \tag{27}$$

Substitution of Equations 26 and 27 into the integral of Equation 25 yields

$$B_T^c(\lambda_c,t) = \int_{\lambda_c-s/2}^{\lambda_c+s/2} B^c(\lambda_c + a\sin\omega_2 t + |X|)T(\lambda_c + a\sin\omega_2 t + |X|)\left[1 - \frac{|X|}{s}\right]\mathrm{d}x \tag{28}$$

A Taylor series expansion may be performed on the terms of Equation 29.

$$B^c(\lambda) = B^c(\lambda_c) + [a\sin\omega_2 t + |X|]B^{c\prime}(\lambda_c) + \frac{[a\sin\omega_2 t + |X|]^2}{2}B^{c\prime\prime}(\lambda_c) + \dots$$

$$T(\lambda) = T(\lambda_c) + [a\sin\omega_2 t + |X|]T'(\lambda_c) + \frac{[a\sin\omega_2 t + |X|]^2}{2}T''(\lambda_c) + \dots \tag{29}$$

where the primes indicate the derivative of the expression with respect to λ evaluated at λ_c. For the purposes of arriving at the desired expression in this derivation, the expansion was only carried to the second order in $[a\sin\omega_2 t + |X|]$. Multiplication of all terms and subsequent integration over the spectral bandwidth results in the expression

$$\begin{aligned} B_T^c(\lambda_c,t) = {} & sBT + \frac{sa^2}{4}[BT'' + 2B'T' + B''T] \\ & + sa[\sin\omega_2 t][BT' + B'T + \frac{a^2}{8}(3B'T'' + 3B''T')] \\ & + \frac{sa^2}{4}[\sin 2\omega_2 t][BT'' + 2B'T' + B''T] \\ & + \text{higher harmonics} \end{aligned} \tag{30}$$

where all superscripts except for the primes have been omitted to simplify the expression.

The first two terms of the expression represent the dc signal output of the multiplier phototube detector.

Of the terms appearing at the fundamental frequency ω_2, the first term (BT') contains the first derivative of the transmitted spectrum and is the term of interest; the second term ($B'T$) contains the first derivative of the source spectrum and is zero if the source radiance is constant or is a constant if the source radiance increases or decreases linearly over the spectral modulation interval, a; the third term ($3a^2/8B'T''$) contains the second derivative of the transmitted spectrum and is zero at the wavelength of the first derivative maximum and the fourth term ($3a^2/8B''T'$) contains the second derivative of the source spectrum and is zero if the source spectrum has no fine structure over the spectral modulation interval.

Of the terms appearing at the second harmonic, $2\omega_2$, the first (BT'') contains the second derivative of the transmitted spectrum, and is the term of interest; the second ($2B'T''$) contains the first derivative of the transmitted spectrum and is zero at the wavelength of the second derivative maximum; the third ($B''T$) contains the second derivative of the source spectrum and is zero if the source spectrum has no fine structure over the spectral modulation interval.

Subject to the above conditions, only two terms in the entire expression are important in the ac detection mode. These are the first term at the fundamental frequency ω_2, *i.e.*,

$$sa[\sin\omega_2 t]B^c(\lambda_c)T'(\lambda_c) \tag{31a}$$

and the first term at the second harmonic frequency $2\omega_2$, *i.e.*,

$$\frac{sa^2}{4}[\sin 2\omega_2 t]B^c(\lambda_c)T''(\lambda_c) \tag{31b}$$

Each of these expressions may be expanded by substitution of the appropriate derivatives.

$$\begin{aligned} T(\lambda) &= \exp[-\bar{k}_\lambda l] \\ T'(\lambda) &= \left(\frac{\mathrm{d}k_\lambda}{\mathrm{d}\lambda}\right)l\exp[-\bar{k}_\lambda l] \\ T''(\lambda) &= \left(\frac{\mathrm{d}^2k_\lambda}{\mathrm{d}\lambda^2}\right)l\exp[-\bar{k}_\lambda l] + \left(\frac{\mathrm{d}k_\lambda l}{\mathrm{d}\lambda}\right)^2\exp[-\bar{k}_\lambda l] \end{aligned} \tag{32}$$

The above expressions may be evaluated by taking the appropriate derivatives of Equation 23, *i.e.*,

$$\frac{\mathrm{d}\bar{k}_\lambda}{\mathrm{d}\lambda} = -\left(\frac{2\rho k_0}{\Delta\lambda^2}\right)[\lambda - \lambda_0]\exp - \left[\frac{\lambda - \lambda_0}{\Delta\lambda}\right]^2 \tag{33a}$$

and

$$\frac{\mathrm{d}^2\bar{k}_\lambda}{\mathrm{d}\lambda^2} = -\left(\frac{2\rho k_0}{\Delta\lambda^2}\right)\exp - \left[\frac{\lambda - \lambda_0}{\Delta\lambda}\right]^2 + \left(\frac{4\rho k_0}{\Delta\lambda^4}\right)[\lambda - \lambda_0]^2\exp - \left[\frac{\lambda - \lambda_0}{\Delta\lambda}\right]^2 \tag{33b}$$

By substituting Expressions 33a and 33b into Expressions 32 and evaluating at λ_c, one obtains

$$T'(\lambda_c) = \left(\frac{2\rho k_0 l}{\Delta\lambda^2}\right)[\lambda_c - \lambda_0] \exp -\left[\frac{\lambda_c - \lambda_0}{\Delta\lambda}\right]^2 \exp[-\bar{k}_\lambda l] \quad (34)$$

and

$$T''(\lambda_c) = \left(\frac{2\rho k_0 l}{\Delta\lambda^2}\right) \exp -\left[\frac{\lambda_c - \lambda_0}{\Delta\lambda}\right]^2 + \left(\frac{4\rho k_0 l}{\Delta\lambda^4}\right)[\lambda_c - \lambda_0]^2 \exp -\left[\frac{\lambda_c - \lambda_0}{\Delta\lambda}\right]^2 + \left\{\left(\frac{2\rho k_0 l}{\Delta\lambda^2}\right)[\lambda_c - \lambda_0] \exp -\left[\frac{\lambda_c - \lambda_0}{\Delta\lambda}\right]^2\right\}^2 \exp[-\bar{k}_\lambda l] \quad (35)$$

The location of the maximum or minimum of Equation 33a can be found by setting Equation 33b to zero, substituting λ_c for λ and solving for λ_c. At the maximum or minimum

$$\lambda_c = \lambda_0 \pm \frac{\Delta\lambda}{\sqrt{2}} \quad (36)$$

The maxima or minima of Equation 35 can be located by setting $\frac{d^3\bar{k}_\lambda}{d\lambda^3}$ equal to zero and solving for λ_c. Three values are obtained, of which $\lambda_c = \lambda_0$ is the maximum.

$$\lambda_c = \lambda_0 \qquad \lambda_c = \lambda_0 \pm {}^3/_2\,\Delta\lambda \quad (37)$$

When Equation 34 is evaluated at $\lambda_c = \lambda_0 + \frac{\Delta\lambda}{\sqrt{2}}$, it becomes

$$T'(\lambda_c) = \left(\frac{2\rho k_0 l}{\sqrt{2}\Delta\lambda}\right) \exp\left[-\frac{1}{2}\right] \exp[-\bar{k}_\lambda l] \quad (38)$$

Evaluating Equation 35 at $\lambda_c = \lambda_0$, one obtains

$$T''(\lambda_c) = \left(\frac{2\rho k_0 l}{\Delta\lambda^2}\right) \exp[-\bar{k}_\lambda l] \quad (39)$$

These expressions may be substituted back into Equations 31a and 31b and Equation 1 substituted for $B^c(\lambda)$. If also only terms with $\omega_1 + \omega_2$ and $\omega_1 - \omega_2$ are retained, then Equation 31a becomes

$$B_T^c(\lambda_c,t) = sa[\sin\ \omega_2 t][B^c(\lambda_c)T'(\lambda_c)] = (\sin\ [\omega_1 + \omega_2]t + \sin\ [\omega_1 - \omega_2]t) \cdot \left[\frac{sa\ B^0(\lambda)\rho k_0{}^l \exp[-\ {}^1/_2] \exp[-\bar{k}_\lambda l]}{2\sqrt{2}\Delta\lambda}\right] \quad (40)$$

Equation 40 predicts that the first derivative of the transmitted spectrum should appear at both the sum and the difference of the modulation frequencies. Similar substitution can be made into Equation 31b with the result being

$$B_T^c(\lambda_c,t) = \frac{sa^2}{4}[\sin\ 2\ \omega_2 t][B^c(\lambda_c)T''(\lambda_c)] = (\sin\ [\omega_1 + 2\omega_2]t + \sin[\omega_1 - 2\omega_2]t) \cdot \left[\frac{sa^2 B^0(\lambda)\rho k_0 l\ \exp[-\bar{k}_\lambda l]}{8\Delta\lambda^2}\right] \quad (41)$$

Equation 41 predicts that the second derivative of the transmitted spectrum should appear at the sum of the chopping frequency and twice the wavelength modulation frequency and also at their difference. The signal expression for the first and second derivatives (refer to Equations 6 and 7) can be obtained by substituting Equations 40 or 41 into

$$S = WH\Omega_M T_f \gamma\ R_L\ B_T^c(\lambda_c,t) \quad (42)$$

where W is the monochromator slit width, in cm, H is the monochromator slit height (assuming equal entrance and exit slits), Ω_M is the solid angle of radiation collected by the monochromator, in sr, T_f is the transmission factor for the entire optical system, γ is the photoanodic sensitivity of the photomultiplier tube, in A W^{-1}, R_L is the resistance of the phototube load resistor, in Ω, as $B_T{}^c(\lambda_c,t)$ is given by Expression 40 for the first derivative signal and by Expression 41 for the second derivative signal.

KEY TO SYMBOLS

a = Lateral displacement of refracted beam, nm
A = Atomic weight, amu
B = Factor accounting for noise contribution from dynodes, no units
$B^0(\lambda)$ = Unmodulated source spectral radiance at wavelength λ, W cm^{-2} sr^{-1} nm^{-1}
$B^c(\lambda)$ = Modulated source spectral radiance at wavelength λ, W cm^{-2} sr^{-1} nm^{-1}
$B_T{}^c(\lambda)$ = Radiance transmitted through flame at wavelength λ, W cm^{-2} sr^{-1} nm^{-1}
$B_T{}^c(\lambda_c,t)$ = Radiance viewed by phototube at wavelength λ_c and time t, W
c = Speed of light, cm sec^{-1}
C^l = Limiting detectable solution concentration, μg ml^{-1}
d = Lateral geometric displacement of refracted beam, cm
e = Electronic charge, 1.6×10^{19} C
E_i = Excitation energy of state i, eV
f = Absorption oscillator strength, no units
Δf = Frequency interval over which amplifier readout system responds, Hz
g_i = Statistical weight of state i
H = Monochromator slit height, cm
$\overline{\Delta i_p}$ = rms noise signal due to the photodetector, A
k = Boltzmann constant, 8.64×10^{-5} eV $°K^{-1}$
$k_0{}^l$ = Peak atomic absorption coefficient for the minimum detectable concentration, cm^{-1}
k_0 = Peak atomic absorption coefficient at λ_0 for pure Doppler broadening, cm^{-1}
$\bar{k}_\lambda$ = Modified atomic absorption coefficient, cm^{-1}
l = Absorption path length of flame, cm
L = Free length of vibrating member of refractor plate assembly, cm
M = Multiplication (amplification) factor of photodetector, no units
n^l = Limiting atomic concentration of species of interest in flame, atom cm^{-3}
$n_i{}^l$ = Limiting atomic concentration of species of interest in state i in flame, atom cm^{-3}
n_T = Number of moles of flame gas products at temperature T, no units
n_{298} = Number of moles of flame gas products at 298 °K, no units
Q = Flow rate of unburned gases, cm^3 sec^{-1}
R_d = Reciprocal linear dispersion of monochromator, nm cm^{-1}
R_L = Phototube load resistor, Ω.
s = Spectral bandwidth of monochromator, nm
$S(\lambda)$ = Slit function of the monochromator, no units
$S_{\omega_1+\omega_2}$ = First derivative signal, V
$S_{\omega_1+2\omega_2}$ = Second derivative signal, V
T = Absolute temperature of flame gases, °K
T_f = Transmission factor of instrumental system of lenses, monochromator and flame, no units
$T(\lambda)$ = Transmission of analyte atoms as function of λ, no units
$|X|$ = $|\lambda - \lambda_c|$, Å.
W = Monochromator slit width, cm
$Z(T)$ = Electronic partition function, no units
α = Angle of beam incident to refractor plate, rad
β = Factor to account for incomplete atom formation (free-atom fraction), no units
γ = Phototube sensitivity factor, A W^{-1}
ϵ = Efficiency of nebulization and vaporization processes (aspiration yield), no units

λ = Any wavelength passing through center of exit slit of monochromator, nm
λ_c = Wavelength passing through center of exit slit when refractor plate is perpendicular to the optical axis of the monochromator, nm
λ_0 = Wavelength at center of absorption line profile, nm
$\Delta\lambda$ = Apparent half-width of absorption line, nm
$\Delta\lambda_A$ = Half-width of absorption line, nm
$\Delta\lambda_D$ = Doppler half-width of absorption line, nm
μ = Refractive index of refractor plate, no units
π = 3.1416...
$\frac{\pi e^2}{mc}$ = 2.65×10^{-2} cm^2 sec^{-1}
ρ = Coefficient to correct k_0 for instrumental broadening, no units
τ = Thickness of refractor plate, cm
ϕ = Flow rate of solution into nebulizer, cm^3 min^{-1}
Ω_M = Solid angle of radiation collected by the monochromator, sr
ω_1 = Frequency of mechanical chopper (source modulation), Hz
ω_2 = Frequency of refractor plate oscillation (wavelength modulation), Hz

RECEIVED for review August 5, 1971. Accepted December 7, 1971. One of the authors (R. C. E.) thanks the Graduate School of the University of Florida for financial support in the form of a Graduate School Fellowship. This work was supported by AFOSR (AFSC), U.S.A.F. Grant 70-1880B.

Flame Detection Method for Determining Organic Carbon in Water

F. T. Eggertsen and F. H. Stross

Shell Development Company, Emeryville, Calif.

Trace organic carbon in water can be determined by means of a thermal analysis-flame detection system previously devised for the thermal stability and volatility characterization of organic materials. In the method developed, a small sample is heated in nitrogen carrier gas in two stages to determine volatile (<150 °C) and nonvolatile (150–550 °C) organic carbon with the hydrogen flame ionization detector. The water evaporated in the first stage changes the detector response to some extent but this is taken care of by calibration. Performance of the method is illustrated in tests with 1 to 300 ppm of various types of organic material. The lower limit of detection is about 0.2 ppm. Advantages of the method are its simplicity and sensitivity and a differentiation of the organic material according to volatility. The analysis time is about 15 minutes.

THE CURRENT EMPHASIS on clean environment has led to great interest in the development of apparatus for determining organic contaminants in water. A type of analysis frequently desired is the measurement of total organic carbon. One of the best known commercial instruments developed for this purpose is the Beckman total organic carbon (TOC) analyzer, which utilizes an analysis scheme developed by Van Hall and coworkers (1). In this scheme of analysis the organic carbon in a water sample is oxidized to CO_2 which is swept through an infrared cell for measurement. Another instrument, introduced recently by the Precision Scientific Company, and based on the work of Stenger and Van Hall (*2*), is the "Aquarator"; in this approach the organic carbon is oxidized to CO by CO_2 carrier gas and the CO is determined by infrared. A more sensitive method, which utilizes a hydrogen flame ionization detector, was introduced by Lysyj *et al.* (*3*, *4*). In this method the water sample is injected into a high temperature pyrolyzer and the organic carbon is determined by sweeping the products to the detector using nitrogen or water vapor as a carrier gas.

The present report describes a method, also utilizing a flame detector, which is simpler is some respects than that of Lysyj and supplies additional information. It is carried out by means of a thermal analysis–flame ionization detection (TAFID) instrument previously developed for thermal stability and volatility measurements of organic materials (*5*, *6*). The analysis is made simply by rapidly vaporizing the water sample under controlled conditions, followed by a second heating stage, while sweeping the vapors with nitrogen carrier gas directly into the flame detector. A particular advantage of the method is that it characterizes the sample according to volatility. Volatile organic material is evolved while vaporizing the water; and the relatively nonvolatile material is obtained by a rapid high temperature pyrolysis step.

The feasibility of using the TAFID type of instrument for this analysis has been reported by Butz *et al.* (*7*). In the present study this approach was investigated in more detail to develop a rapid quantitative method.

EXPERIMENTAL

Apparatus. A schematic diagram of the system is shown in Figure 1. The basic components include the following. A sample furnace, of Vycor tubing, heated by resistance wire winding, FID detector, modified Aerograph, the flame jet of which is also of Vycor and sealed to the sample furnace, capable of operation at 500 °C; amplifier, Aerograph electrometer 500-D; furnace heating controls, manual control by suitable adjustment of voltage (potentiometer) to the heater windings, or a temperature programmer; integrator, digital

(1) C. E. Van Hall, J. Safranko, and V. Stenger, ANAL. CHEM., **35**, 315 (1963).
(2) V. Stenger and C. E. Van Hall, *ibid.*, **39**, 206 (1969).
(3) I. Lysyj, K. H. Nelson, and P. R. Newton, "Methods for the Determination of Trace Organic Materials in Water," U.S. Dept. of the Interior, Office of Saline Water, Research and Development Progress Report No. 239, February, 1967; *J. Water Pollut. Contr. Fed.*, **41** (5), Pt. 1, 831 (1969).
(4) K. H. Nelson, I. Lysyj, and J. Nagano, *Water Sewage Works*, **117**, 14 (1970).
(5) F. T. Eggertsen, H. M. Joki, and F. H. Stross, "Thermal Analysis," Vol. 1, R. F. Schwenker, Jr., and P. D. Garn, Ed., Academic Press, New York, N.Y. 1969, p 341.
(6) F. T. Eggertsen, E. E. Seibert, and F. H. Stross, ANAL. CHEM., **41**, 1175 (1969).
(7) W. H. Butz, A. C. Stapp, and Alan Di Stefano, "Total Organic Content (TOC) Analysis with a New FID Thermal Analyzer," presented at the Pittsburg Conference on Analytical Chemistry and Applied Spectroscopy, Cleveland, Ohio, March 1970.